Blooming in H2RG arrays: laboratory measurements of a second brighter-fatter type effect in HgCdTe infrared detectors

Gregory R. Zengilowski[a,*] **Mario S. Cabrera**[b] **Craig W. McMurtry**[a] **Judith L. Pipher**[a] **Meghan L. Dorn**[c] **Nicholas S. Reilly**[a] **Danielle Bovie**[a] **Amy K. Mainzer**[d] **Andre F. Wong**[d] **and Donald Lee**[c]

[a]University of Rochester, Department of Physics and Astronomy, Rochester, New York, United States

[b]Conceptual Analytics LLC, Glenn Dale, Maryland, United States

[c]Teledyne Imaging Sensors, Camarillo, California, United States

[d]University of Arizona, Lunar and Planetary Sciences Laboratory, Tucson, Arizona, United States

Abstract. Improved measurement and calibration of detector behaviors will be crucial for future space missions, particularly those aiming to tackle outstanding questions in cosmology and exoplanet research. Similarly, many small detector effects, such as the nearest-neighbor interactions of the brighter-fatter effect and interpixel capacitance, will need to be considered to ensure measured signals are truly astronomical in origin. Laboratory measurements confirming the existence of an additional brighter-fatter type effect in HAWAII-1RG and HAWAII-2RG HgCdTe infrared arrays with cutoff wavelengths ranging from 5.7 to 16.7 μm are presented. This effect is similar in nature to the blooming observed in charge-coupled devices and is characterized by a pixel spontaneously sharing a current with its neighbors upon reaching saturation, serving to make the brightest sources appear fatter. In addition to exploring the cause and mechanism of current sharing for this effect, measurements for several arrays show the magnitude of the shared current is greater than 60% of the incoming photocurrent hitting the saturated pixel. A proof-of-concept correction method for this effect is also described along with the necessary next steps to improve this correction and investigate the amplitude of other nearest-neighbor interactions. [DOI: 10.1117/1.JATIS.7.2.026002]

Keywords: HgCdTe; nearest-neighbor interactions; long wavelength infrared; midwave infrared; infrared detector; brighter-fatter effect.

Paper 21019 received Feb. 5, 2021; accepted for publication May 20, 2021; published online Jun. 4, 2021.

1 Introduction

Future space missions designed to characterize the atmospheres of exoplanets will require both extremely precise differential photometry and a strong understanding of undesirable detector behaviors because of the small targeted signals. An Earth-sized planet transiting a solar-type star would cause a drop in white light intensity of 0.0084% ($R^2_{\text{planet}}/R^2_{\text{star}}$) and finding any chemical constituents within the atmosphere of this planet would require discerning small wavelength variations in this already minuscule signal. Early studies will likely focus on cooler M-type host stars where, due to the smaller stellar radii, the dip in intensity for a transiting planet would be larger. For example, the same Earth-like planet transiting an M8 star would cause a dip in white light intensity of 1%. As a result, detector behaviors must be studied and calibrated to well below the 1% level to ensure any measured variation in transit depth is astronomical in origin, rather

*Address all correspondence to Gregory R. Zengilowski, g.zengilowski@rochester.edu

2329-4124/2021/$28.00

than arising from a deviation from the simplified model of a discrete lattice of independent pixels perfectly slicing the input image.

A few such deviations from this idealized picture fall into the category of nearest-neighbor interactions, where the signal value read in a pixel is coupled to the signal values of its neighbors through a variety of mechanisms. There are two previously identified nearest-neighbor interactions in the popular HAWAII-xRG (HxRG) format HgCdTe arrays produced by Teledyne Imaging Sensors (TIS), where the x in HxRG denotes the size of the array. The first nearest-neighbor interaction is known as interpixel capacitance[1] (IPC), where a pixel is capacitively coupled to its neighbors. When the voltage across a central pixel changes, so too does the electric field around it. If this field overlaps with the electric field of its neighbors, which occurs in the epoxy between the detector layer and the readout circuitry, the changing electric field drives a displacement current in the neighboring pixel. As a result of this capacitive coupling, some fraction of the voltage change generated by a central pixel collecting charges is instead measured in its neighbors.

The brighter-fatter effect, which is characterized by brighter sources appearing larger in spatial extent, or "fatter" than dimmer sources, is the second commonly referenced nearest-neighbor interaction. Although originally noticed[2] in charge-coupled devices (CCDs), it has also been observed[3] in HxRG arrays. For these arrays, the brighter-fatter effect is proposed[4] to be caused by unequal lateral diffusion of charges among a bright pixel and its dimmer neighbors, as opposed to the capacitive voltage sharing that drives IPC signal sharing. Photogenerated charges randomly walk through the HgCdTe detector material until either being lost through recombination or encountering the depletion region around a p-n junction that defines each pixel, a diagram of which is shown in Fig. 1. Upon entering the depletion region, the charge is swept across the junction by the local electric field and collected by the pixel. As a pixel accumulates charge, the depletion region around it shrinks. A charge generated at the midpoint between a bright pixel, with a small depletion region, and a dim neighbor has a higher probability of randomly walking to the larger depletion region of the dimmer neighbor leading to a net outward, diffusive flow away from the bright central pixel, making the image fatter.

Laboratory measurements investigating an additional nearest-neighbor interaction are presented. The behavior of this interaction is similar to the brighter-fatter effect, in that it makes

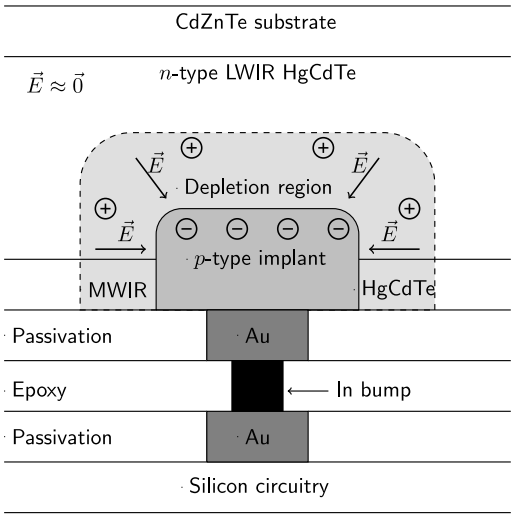

Fig. 1 A basic block diagram of a LWIR H2RG pixel. The size and shape of each region are intentionally drawn not to scale for ease of identifying each component. When a photon is absorbed in the LWIR HgCdTe detector material, it generates an electron–hole pair. These charges randomly walk through the detector layer until either recombining or encountering the depletion region. If a hole reaches the depletion region, it is swept across the junction by the electric field. In the process of moving a positive charge from the positively charged side of the junction to the negatively charged side, the magnitude of the separated charges is reduced. As a result, the depletion region width decreases, as does the electric field and thus the voltage across the junction.

the brightest sources appear fatter through unequal lateral diffusion but with a different source of the shared charges. To distinguish between these two effects, the original brighter-fatter effect will be labeled here as brighter-fatter 1 (BF1), and this new effect will be labeled brighter-fatter 2 (BF2). Where the original BF1 contributes over the full dynamic range of a pixel, BF2 has a specific, repeatable onset that coincides with the bright pixel reaching saturation. At this point, charges begin to spill out of the saturated central pixel into its neighbors causing an outward blooming of the signal. This behavior is similar in nature to the blooming observed when pixels in CCDs saturate, albeit with a slightly different end result and caused by an entirely different mechanism.

Because BF2 begins to occur as pixels approach saturation, the bulk of its influence can be avoided by intentionally operating far from full well depth. There are some cases, however, where avoiding it entirely will be inescapable, and it becomes more prevalent in longer wavelength HgCdTe detectors, such as the 10.5-μm cutoff wavelength arrays to be used in the long wavelength infrared (LWIR) channel of the Near-Earth Object Surveyor (NEO Surveyor), a NASA mission currently in the formulation phase. The HgCdTe detector layer is grown on a CdZnTe substrate, requiring fine-tuning of the substrate lattice spacing. Growing on substrates with different lattice spacing than the bulk material causes strain within the detector layer, which is released through defects.[5] Appropriately matched substrates can reduce the defect density observed in HxRG arrays.

Altering the mercury-cadmium ratio in HgCdTe materials changes the cutoff wavelength, with smaller cadmium fractions corresponding with longer cutoff wavelengths. Because of the relatively weak HgTe bonds,[6] longer wavelength HgCdTe is softer than shorter wavelength equivalents and as a result is more susceptible to strain-related defects that facilitate egregious trap-assisted tunneling dark currents. As these tunneling currents are bias dependent, they have a large initial magnitude immediately after resetting the array. While holes are collected and the bias decreases during an integration, these tunneling currents decay producing a characteristic curvature in signal versus time data. In the long wavelength arrays to be used with NEO Surveyor, the number of pixels exhibiting initial tunneling currents greater than 200 e-/s, including many that saturate from their own dark current within the planned integration times for this mission and thus participate in BF2 sharing, is on the order of 10% or less of the full array.

Assuming, for simplicity, that one of every 10 pixels is susceptible to sharing charge through BF2, any average pixel is likely to feel the influence of BF2 either as the central pixel sharing charge or receiving charge from one of its eight nearest neighbors. Because a typical point spread function (PSF) does not involve only a single pixel, it is even more likely that an average PSF will be vulnerable to this effect. Furthermore, because the strain-related defects occur predominantly along crosshatching lines, which occur at the intersections of the (211) growth plane and the eight HgCdTe slip planes,[7] the presence of this effect is likely to be more dominant in certain localized sections of the array. This can be especially problematic for spectroscopic missions, including those focusing on characterizing exoplanet atmospheres, where BF2 could appear as a systematic brightening of specific wavelengths. This behavior would potentially obscure any desired transit depths at these wavelengths even if the central inoperable pixels are masked to avoid their contribution. Masking the eight immediate neighbors of a BF2 sharing pixel to avoid the influence of this effect requires increasing the total inoperable area of the array by a factor as large as 9, making it significantly more desirable to focus on study and calibration of BF2 than to attempt to avoid its impact.

2 Sampling and Calibration

During testing, the arrays being analyzed are operated in a low pressure (<1 mTorr) dewar cooled with liquid helium and liquid nitrogen and held to a stable temperature using resistive heaters and a Lake Shore Cryotronics temperature controller. A room temperature piece of high emissivity black felt is used as the light source and the light passes through a ZnSe window on the dewar and an internal filter wheel that houses two circularly variable filters (CVFs) covering the wavelength range of 4 to 14 μm in addition to several discrete filters before striking the

detector. There is also a cold dark shutter in this filter wheel designed to block light producing nonilluminated conditions with a light leak well below[8] 1 e-/s at LWIR wavelengths.

Each read of the array shows the voltage measured across every pixel and the produced images are used here with two primary sampling methods. In the first method, known as correlated double sampling[9] (CDS), the array is read twice nondestructively with a set integration time between the two reads. The resulting CDS image is the difference between the two frames, which shows the net voltage change across the integration time for each pixel. The second method, which is known as sample-up-the-ramp[10] (SUTR), involves reading the array multiple times at equally spaced time-steps over a long integration time. The first read in the ramp is known as the pedestal frame and is subtracted from every subsequent frame to serve as a baseline zero-point for the integration. This method allows for study of the evolution of a pixel's behavior as it accumulates charge through a prolonged integration or in response to varying conditions.

Although reading an array with these methods shows voltage changes across an integration, most end users of HxRG detectors require knowing the number of charges collected during that time period. This requires measuring a conversion factor with units of charge/volt, which is a capacitance, to translate the observed voltage changes into accumulated charges. The noise squared versus signal method[11] is typically used to measure the capacitance. An extra correction is needed for this method to account for a blurring of the image caused by IPC, which reduces the noise without altering the signal for uniform illumination patterns.[1] For this work, the IPC correction factor is measured using the hot pixel method.[12] In addition, the capacitance increases as pixels accumulate charge because of the decreasing depletion region width. Using a constant capacitance value can lead to underestimating the total number of collected charges by up to 10%. The resulting signal nonlinearity can be measured using the flux versus fluence method.[13] Typical values for the capacitance are around 2 e-/ADU and values for the signal nonlinearity are about -2.5×10^{-6} 1/ADU for 250 mV of applied bias, where 1 ADU (analog-to-digital unit), which is a convenient measure for voltage, represents a change of 7.7 μV across a pixel.

3 Detecting Brighter-Fatter 2

BF2 can be easily detected by sampling a large SUTR set with an integration time long enough to allow certain pixels to saturate prior to their neighbors. Several examples of BF2 are shown in Fig. 2, where as one pixel saturates, each[13] of its neighbors sees a spontaneous increase in the signal rate as if an extra current source is switched on and sent to the neighboring pixels. This experiment is performed in the dark to eliminate the sharing being caused by an interaction with the photocurrent, such as is seen with BF1. If the source of the extra current causing the signal rate increase is the saturated pixels themselves, then a neighboring pixel should see an instantaneous increase in the slope of signal versus time data at the moment a neighbor saturates from dark current alone. This behavior is precisely observed. Signal versus time data are shown in Fig. 2(a) for neighboring pixels in the dark in a 10-μm cutoff H2RG array. At the moment the high dark current pixel reaches saturation (vertical dashed line), the neighboring pixel observes an instantaneous increase in incoming signal rate as the net current entering the pixel spontaneously increases. Figure 2(b) shows the signal versus time data for another pixel in this same array, which exhibits multiple changes of slope before saturating. Each of the three changes in slope corresponds exactly with one of its neighbors saturating due to dark current alone. This behavior is not exclusively a 10-μm or a 40-K issue, as the same behavior can be seen in a 5.7-μm cutoff H2RG array at 77 K in Fig. 2(c) and in a 16.7-μm cutoff H1RG array at 23 K in Fig. 2(d).

With the onset of BF2 occurring when a neighboring pixel approaches saturation, it is worth briefly reviewing what causes pixels in these arrays to saturate. Every light-reactive pixel in an HxRG array is a photodiode and the diode diffusion dark current of these pixels can be modeled by the Shockley ideal diode equation as[14]

$$I = I_0\left(e^{\frac{qV}{k_bT}} - 1\right) = I_0\left(e^{\frac{V}{V_T}} - 1\right), \tag{1}$$

where I_0 is the magnitude of the small dark current measured under reverse bias, V is the actual voltage across the diode, and a conventional current of positive charge carriers flowing from the

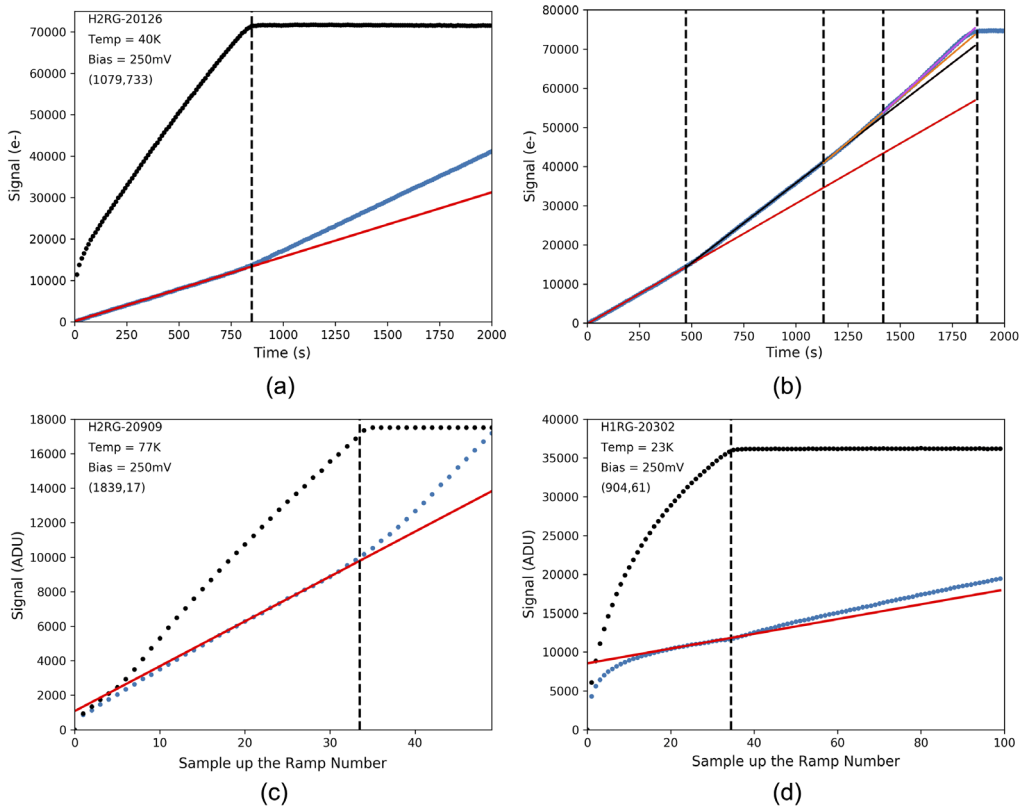

Fig. 2 The spontaneous increase in signal rate associated with BF2 measured in the dark for a variety of detector types and temperatures coincides with a neighboring pixel saturating. In each figure, the vertical dashed lines represent a pixel saturating. (a) Signal versus time data for a pixel (blue) in the 10.2-μm cutoff wavelength array H2RG-20126 at $T = 40$ K show a spontaneous increase in signal rate, depicted as the change in slope, at the exact moment one of its neighbors (black) saturates. The red line shows the initial signal rate carried through to make the change easier to identify. (b) A pixel, also from H2RG-20126, that exhibits multiple changes in slope caused by BF2. Each increase coincides with one of its neighbors saturating (vertical dashed lines). The colored lines show the signal rates of each region and are carried through to make the changes easier to identify. BF2 is also measurable in other arrays, such as (c) H2RG-20909, a 5.7-μm cutoff array, at $T = 77$ K and (d) H1RG-20302, a 16.7-μm cutoff array, at $T = 23$ K. The black curve in (a) and both curves in (d) exhibit the characteristic curvature caused by bias-dependent tunneling currents that decay as the voltage across the pixel decreases throughout the integration.

p-type implant to the n-type bulk is defined as positive in this convention. V_T is known as the thermal voltage and is 3.45 mV at 40 K. Due to the small thermal voltage, this current is essentially the small constant I_0 when operating under reverse bias ($V < 0$) and increases exponentially as the pixel approaches and enters forward bias ($V > 0$). The absorption of photons drives a conventional current flowing from the n-type bulk to the p-type implant, which pushes the pixels from their initial reverse bias voltage toward forward bias. Given enough time and a large enough photocurrent, these pixels will continue to accumulate charge until eventually reaching a final equilibrium voltage, known as saturation. This equilibrium occurs at a voltage when the net outgoing current described in Eq. (1) is equal and opposite to the incoming photocurrent, giving a net zero current flowing through the pixel.

This behavior is depicted graphically in Fig. 3 where each line shows the net current flowing through a pixel. During detector operation, a nonilluminated pixel is initially set into reverse bias and slowly debiases from the small dark current before eventually reaching saturation at the zero bias level ($V = 0$) where the net current through the pixel decays to zero. There is not a complete cessation of movement of charges at this point, but an equal stream of charges flowing in opposite directions across the junction. Under illuminated conditions, the net current curves are

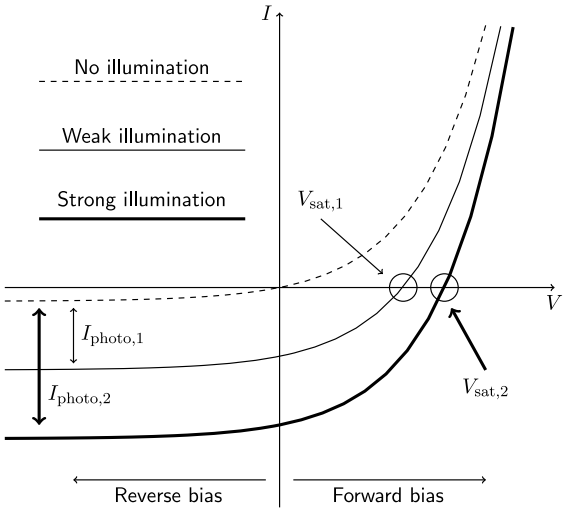

Fig. 3 The $I - V$ characteristics of an illuminated and nonilluminated photodiode. The currents plotted are the net current, with a positive value defined as a conventional current of positive charge carriers flowing from the *p*-type implant to the *n*-type bulk material. These detectors measure minority carriers flowing from the *n*-type to the *p*-type material, so a photocurrent is marked as a negative contribution to the net current behavior, shifting the dashed nonilluminated current down by a magnitude I_{photo}. HxRG detectors are operated under reverse bias and move toward forward bias throughout the integration period. As a pixel approaches forward bias, the outgoing diode current increases exponentially until it is opposite the photocurrent and equal in magnitude. This gives a net current of zero, and a final equilibrium position, known as saturation, is reached. The voltage that saturation occurs at, V_{sat}, depends on the magnitude of the photocurrent, with a larger photocurrent leading to a larger saturation voltage because the outgoing current must be larger to counteract the incoming photocurrent.

shifted down by the photocurrent I_{photo} and the resulting saturation voltage V_{sat} shifts further into forward bias as the photocurrent increases.

Already saturated pixels can also shift between different saturation levels in response to changing illumination levels in an attempt to alter the outgoing current to match the newly changed incoming current. An example of this behavior is shown in Fig. 4 where signal versus time data are shown for a pixel that initially starts in the dark before being placed in the light, at frame 200, and then returned to the dark, at frame 250, without resetting the array. Responding to the changing incoming signal rate, the pixel moves from its first saturated position it reached from dark current alone to a higher saturated position in forward bias as the incoming current instantaneously increases when the array is illuminated, before decaying toward the initial saturation voltage when placed back in the dark. This pixel, however, does not quite reach the initial saturation level. Instead, it finds a new equilibrium slightly into forward bias.

The instantaneous increase in the signal rate of a pixel neighboring a saturated pixel is easily explained by a sudden increase in the physical incoming current entering a pixel. Similarly, the difference between the two dark saturation levels in Fig. 4 can also be explained by such a phenomenon. This is demonstrated by the $I - V$ curves in Fig. 5, which follow the central pixel throughout the different stages of the ramp. A graphical description of where BF2 sharing occurs at each stage of the integration is shown in Fig. 6. For the first 75 frames of the ramp, in stage 1, all of the pixels are in the dark and there is no sharing through BF2, as shown in Fig. 6(a). At about frame 75, the central pixel reaches saturation and enters stage 2 where, as shown in Fig. 6(b), only the central pixel shares current with its neighbors through BF2. At frame 200, a light source is turned on providing a negative current contribution. The central pixel's equilibrium is disturbed [path (b) in Fig. 5] and it shifts into forward bias until reaching a new equilibrium [path (c) in Fig. 5] when the outgoing current has increased to be equal and opposite to the new incoming photocurrent. At this point, stage 3 shown in Fig. 6(c), all pixels are saturated, so all share current with each other through BF2. Finally, at frame 250, the light source is turned off, removing a negative current contribution [path (d) in Fig. 5]. Because the net current

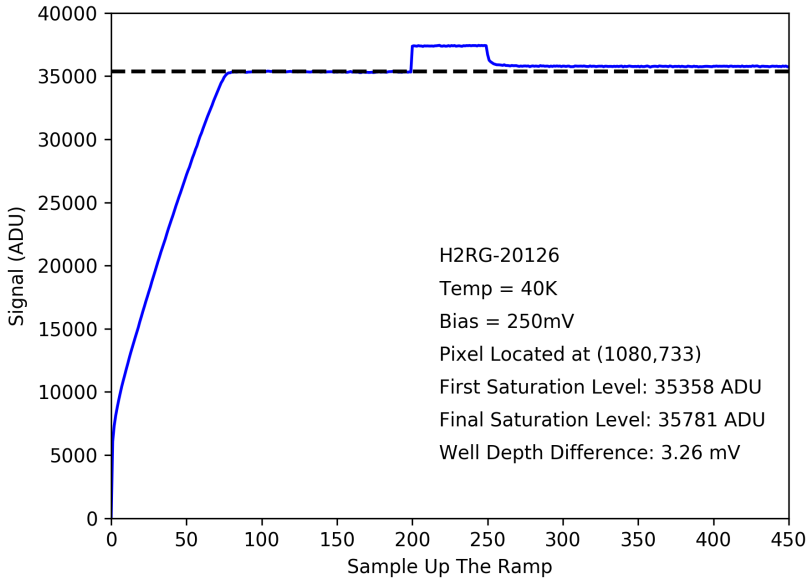

Fig. 4 Signal versus time data for a pixel with sufficient dark currents to saturate in the dark. After saturating in the dark, the pixel is illuminated and put into forward bias, and then is placed back in the dark to decay to zero bias. Because all of the neighbors of this pixel are saturated when placing the array back in the dark, they share current to this pixel through BF2, and the new equilibrium reached is slightly in forward bias.

is now positive, the central pixel decays toward zero bias [path (e) in Fig. 5] until the outgoing current decreases to again be equal and opposite to the incoming current. As seen in Fig. 6(d), during stage 4 all pixels are sharing current through BF2 with each other. As a result, the incoming signal rate entering the central pixel is larger at this point than it was prior to illuminating the array and the voltage does not decay back to zero bias. Instead, a new equilibrium is established slightly in forward bias so the outgoing current can oppose the influence of the new source of shared current. The difference between the two saturation levels in Fig. 4 is approximately the thermal voltage $\frac{kT}{q} = 3.45$ mV, which is the exponential scale constant for the outgoing current, as seen in Eq. (1).

With both of these behaviors explainable by an increase in the physical incoming current to a pixel and with the source of this excess current coming from the neighboring pixels themselves instead of interactions with a photocurrent, the most likely source is the outgoing current, described in Eq. (1), that increases exponentially as a pixel approaches saturation. Under this theory, if the outgoing current decreases, the amount of sharing should also decrease. To test this, a pinhole mask was placed on the surface of H2RG-18235, a 10.2-μm cutoff array, to allow for the saturation of a few pixels at the center of the pinhole while preventing those at the edge from saturating. An example CDS image taken using the pinhole mask is shown in Fig. 7(a).

After exposing the pinholes to a bright flux to saturate a few central pixels in forward bias, the light was turned off allowing the voltage across the saturated pixels to decay to the zero bias level, following the behavior shown in Fig. 4. After the light is blocked by the cold dark shutter, if the sharing is tied to the outgoing current, an unsaturated neighbor should see an exponential decay in signal rate, appearing as a decreasing slope in signal versus time data, with the same time constant as the decrease in signal exhibited by the saturated pixel. The signal versus time data for the unsaturated neighbor should also decay to a linear dark current behavior once the saturated pixel returns to the zero bias level. The result of this experiment is shown in Fig. 7(b), where the predicted behaviors are clearly observed, confirming the sharing is tied to this outgoing current.

As for the mechanism behind the sharing of this outgoing current, there are at least two possible explanations, which are a bit challenging to disentangle. The first possibility is that the pixel is operating as a light-emitting diode (LED), emitting light at the *p-n* junction as streams of holes and electrons radiatively recombine, and this light is then absorbed and collected

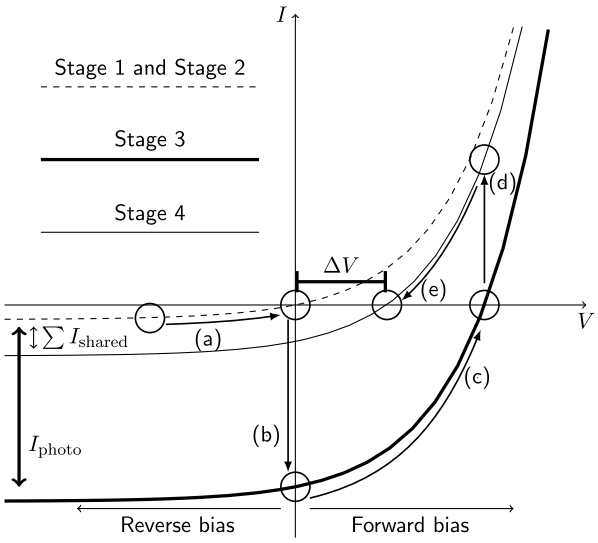

Fig. 5 A series of $I - V$ curves showing the net current through a pixel to explain the different saturation levels in Fig. 4. This diagram uses the sign convention that a negative net current pushes a pixel along a curve in the direction of forward bias and a positive net current toward reverse bias. An equilibrium is reached when the net current is zero, and the pixel will remain at that location on the $I - V$ curve until disturbed by an outside force. Each part of the process is described by an arrow marked with a letter. (a) The pixel starts in the dark at an applied reverse bias and moves toward an equilibrium at zero bias as it debiases from dark current alone. As an important note, the path marked here through $I - V$ space is accurate for most well-behaved pixels, which the pixel shown in Fig. 4 clearly is not. The specific nature of its motion from reverse bias to zero bias is not important, however. Once saturated, this pixel begins sharing current through BF2 with its neighbors, none of whom reciprocate as they are all unsaturated at this point. (b) A saturating light source is turned on, instantaneously providing a negative current contribution to the overall behavior. (c) Because the net current is now negative, the central pixel shifts into forward bias until reaching a new equilibrium with a zero net current. (d) The light source is turned off, removing a negative current contribution. The net current into the central pixel does not return to that seen at the end of step (a), because now all neighbors are saturated and sharing current through BF2. Instead, the central pixel still sees an external incoming signal rate of $\sum I_{\text{shared}}$. (e) Because the net current is now positive, it moves in the direction of reverse bias until reaching a new equilibrium with a net zero current. The final equilibrium voltage is larger than at the end of step (a) and this voltage difference, ΔV, is the 3.26 mV difference seen in Fig. 4.

in an adjacent pixel. The second potential cause is that the stream of holes moving from the p-type implant to the n-type bulk diffuse over to their neighbors where they are swept up by the electric field in the neighbor's depletion region and collected. Neither hypothesis can be definitively eliminated, but one mechanism is more likely due to the material properties of HgCdTe.

The average distance a minority carrier travels before recombining in these arrays, otherwise known as the diffusion length, is on the order[15] of 15 to 20 μm, which is comparable to the center-to-center distance of 18 μm between pixels. The diffusion lengths for the specific arrays used here are considered proprietary information by TIS but are slightly larger, falling within the range of 20 to 50 μm. This suggests holes, on average, are likely to travel the full distance between depletion regions before recombining, particularly in the arrays presented here with diffusion lengths longer than the pixel pitch. Furthermore, as shown in Fig. 8, the measured quantum efficiency (QE), which expresses the fraction of incoming photons successfully detected by an array, is quite close to the theoretical maximum caused by reflection of light as it enters the substrate and detector layers. This suggests loss of charges due to recombination is a very small contribution to the overall behavior.

If, in this chaotic post-saturation environment, recombination becomes a larger contributor, the dominant recombination mechanisms in LWIR HgCdTe at these temperatures are[16–18] Auger 1 recombination and Shockley-Read-Hall recombination. These recombination methods are both nonradiative, where the excess energy is transferred to a third charge carrier or released as a

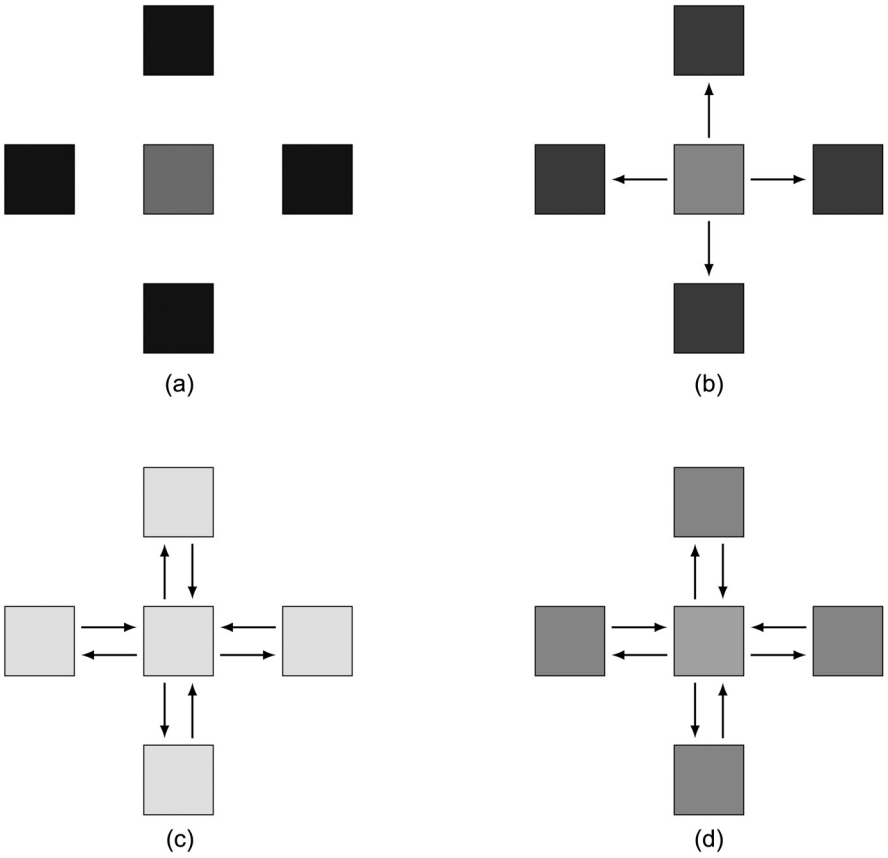

Fig. 6 Block diagrams showing BF2 sharing in different stages for the pixel shown in Fig. 4 to explain the difference between the two saturation levels in the dark. For simplicity, diagonal interactions are ignored. Arrows show sharing through BF2 and the color of each pixel denotes its accumulated signal. (a) Stage 1: All pixels are in the dark and the central pixel has not yet reached saturation from dark current alone. As no pixels are saturated, there is no sharing through BF2. (b) Stage 2: All pixels are still in the dark, but the central pixel has saturated. Because it is the only saturated pixel, the central pixel is the only source of current sharing through BF2, and each of its neighbors sees an instantaneous increase in signal rate. (c) Stage 3: All pixels are strongly illuminated and saturate in forward bias as a result of the large incoming photocurrent. Because all pixels are saturated, they all share current with each other through BF2. (d) Stage 4: The pixels are placed back in the dark and the voltages decay toward zero bias. Because all of these pixels are still saturated, they still share current through BF2. As a result, the incoming external signal rate entering the central pixel does not decay to the same value as seen in stage 2 (b), but instead is the slightly larger value $\sum I_{\text{shared}}$. Accordingly, the voltage of the central pixel does not decay to the same value seen in stage 2 but ends at a slightly larger value. This difference in voltage is the 3.26 mV difference observed in Fig 4.

phonon instead of a photon. Despite not being a dominant recombination process, radiative recombination can occur but is expected to occur at levels an order of magnitude[19] smaller than other recombination mechanisms.

Further limiting the expected contribution of radiative recombination is a proprietary TIS energy gradient that pushes holes toward the *p*-*n* junction and, in the process, also pushes electrons away from the junction to a metal contact near the substrate. This design is used to improve the QE by directing the holes to be collected, rather than relying on random walks, and reducing instances of recombination. In addition to partially preventing recombination, by pulling electrons away from the depletion region, the outgoing current is expected to be dominated by a flow of holes from the *p*-type implant to the *n*-type bulk region rather than electrons flowing in the opposite direction.

One potential explanation that can be eliminated is that this behavior could be caused by photoemissive defects[20] (PEDs). These defects, which occur in the readout not the detector layer,

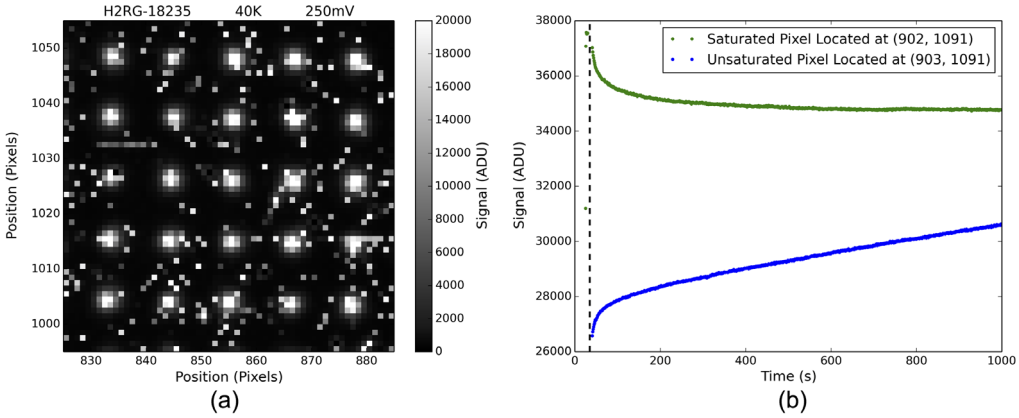

Fig. 7 (a) An example CDS image showing the repeating lattice of pinholes used to confirm BF2 sharing is tied to the outgoing diffusion current. (b) Signal versus time data for a saturated pixel, in green, and one of its unsaturated neighbors, in blue. Using pinholes, a pixel near the center is saturated in the light, keeping its neighbor unsaturated, before blocking the light with a cold dark shutter, which occurs at the vertical dashed line. As the saturated pixel decays from forward bias to the zero bias level, the unsaturated neighbor exhibits a decay in signal rate, exhibited by the decreasing slope, before reaching the expected linear behavior when the saturated pixel reaches the zero bias level. The time constant is matched for the decrease of the outgoing current in the saturated pixel and the decrease in the signal rate of its unsaturated neighbor, suggesting they are related. This serves as strong supporting evidence for the sharing of this outgoing saturation current with neighbors of a saturated pixel.

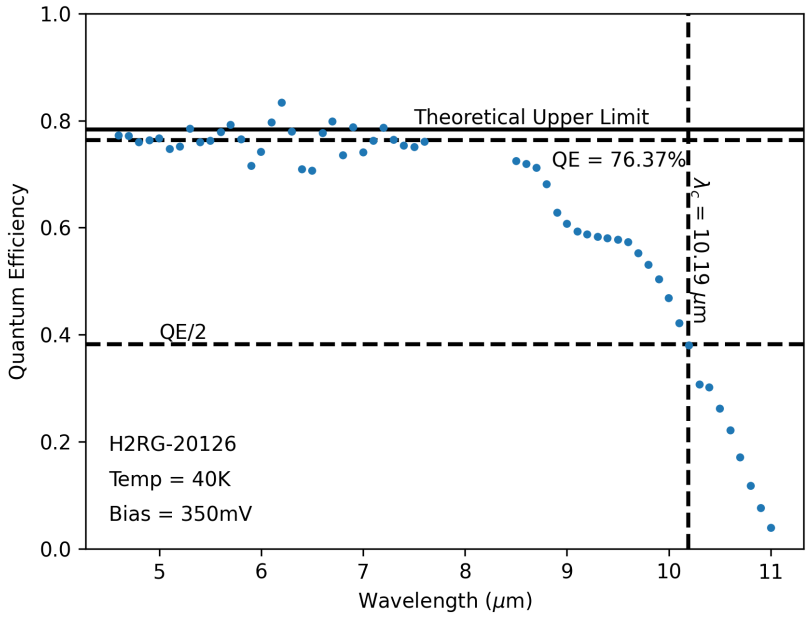

Fig. 8 Measurement of the QE for H2RG-20126, an engineering-grade array that is not antireflection coated, using the two CVFs in the internal filter wheel. QE is measured by comparing the detected number of photons to a theoretical estimate based on parameters such as the bandwidth and transmission of the filters and the blackbody curve of the light source. The overall QE value, top dashed line, is slightly below the theoretical maximum, solid line, caused by the reflection of light as it enters the substrate and detector layers. This suggests loss of charges due to recombination is a small contributor to the overall behavior of the array. The cutoff wavelength of the array is determined by locating the half-power point, which for this array occurs at 10.2 μm.

appear independent of the bias across a pixel, are seen immediately after resetting the array and contribute throughout the integration, and are typically large ($\sim$100 + pixels) in extent. Furthermore, neither of these arrays show any evidence of PEDs, which are repeatably localized, in normal operation. In addition, a PED would be unable to explain a typically well-behaved pixel spontaneously sharing current under certain illuminated conditions, such as is shown in Fig. 7(b). As a result, a PED can be eliminated as a potential source of the current sharing in BF2.

Although the sharing of this outgoing current could be caused by electroluminescence, because of the evidence against radiative recombination being a large contributor to the overall behavior of HgCdTe arrays, it is more likely that the cause of sharing through BF2 is diffusion of the outgoing stream of holes that increases as the depletion region shrinks. Even though neither option can be definitively eliminated, amplitude measurements can provide further support for one cause over another. Finding a large percentage of the outgoing current is shared between neighbors, for example, would support diffusion as the mechanism of sharing because of the expected small number of radiative recombination events.

4 Amplitude Measurements and BF2 Correction

At its core, the amplitude measurement process is quite simple, but several special cases need to be avoided to ensure sharing from only a single pixel is being measured. The basic idea of the method is to determine the incoming current entering a pixel before it saturates by measuring the signal rate and then to compare this measured value to the net change in signal rate of all neighboring pixels before and after the central pixel saturates. The outgoing current should be equal to the incoming current at saturation, and comparing the net excess current I_{excess} sent to each of the neighbors with the measured outgoing current of the central pixel gives a percentage of the outgoing current shared with the nearest neighbors.

To ensure only one pixel is contributing to the measurement, any pixel for which the sharing is measured must saturate first within the 5×5 pixel box around it, and the samples included for measurement end the moment any other pixel within this box saturates. Any pixel of interest must also take long enough to saturate so there are plenty of frames before saturating to determine the presaturation signal rate and saturate quickly enough to ensure there is a sufficient number of frames after saturating to measure the signal rate in the neighbors.

The excess current being sent to the i'th neighbor of a saturated pixel through BF2 can be calculated as

$$I_{\text{excess},i} = I_{\text{post},i} - I_{\text{pre},i}, \tag{2}$$

where $I_{\text{pre},i}$ and $I_{\text{post},i}$ are the slope of the signal versus time data of the i'th neighbor before and after the central pixel saturated, respectively. For a graphical description of these terms, $I_{\text{pre,i}}$ is the slope of the red line in Fig. 2(a) and $I_{\text{post,i}}$ is the slope of the blue points after the vertical dashed line in the same figure. Adding up the individual contributions, the net current being shared by the central pixel can be expressed as

$$I_{\text{BF2}} = \sum_{i=1}^{8} I_{\text{excess},i}, \tag{3}$$

where the sum covers the eight neighboring pixels surrounding the central pixel.

For ease of comparison, describing the amount of sharing in terms of the percentage of the outgoing current shared is often more convenient. This can be accomplished as

$$\text{BF2}[\%] = 100\% \times \frac{I_{\text{BF2}}}{I_{\text{out}}}, \tag{4}$$

where I_{out} is the expected outgoing current from the central pixel. In Fig. 2(a), I_{out} is the slope of the linear portion of the black points prior to saturation and after the initial curvature caused by decaying tunneling currents fades away. The results of this measurement method using long SUTR sets with dim illumination for H2RG-20126 and H2RG-18693 are shown in Fig. 9, where

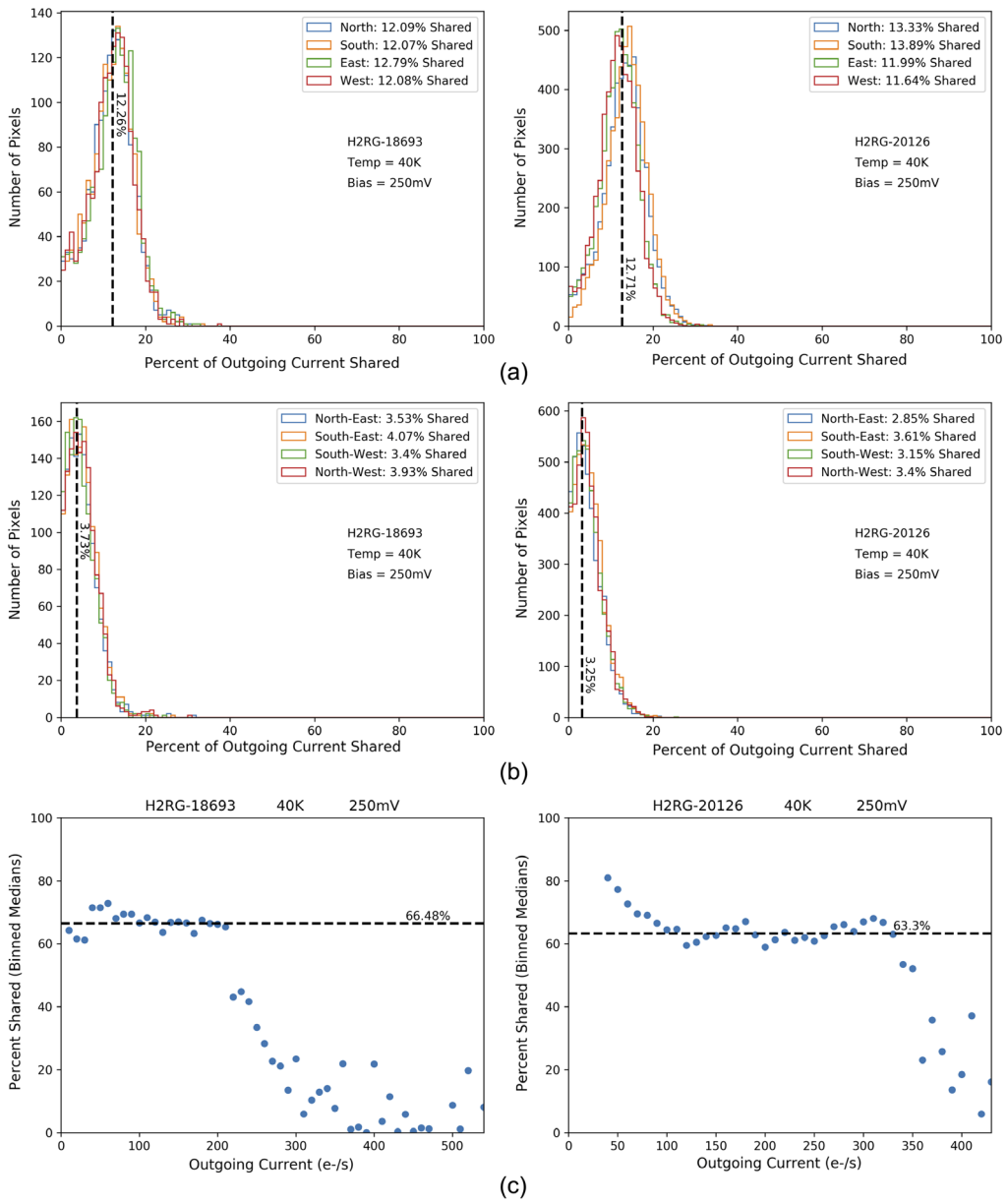

Fig. 9 Result of the BF2 amplitude measurement method for H2RG-18693, left, and H2RG-20126, right. Histograms of the outgoing current shared to (a) direct neighbors and (b) diagonal neighbors. (c) Total percentage shared to all nearest neighbors as median of 10 e-/s wide bins.

8549 central pixels were analyzed for H2RG-20126, right, and 5128 central pixels were analyzed for H2RG-18693, left. A dim constant flux over a long SUTR set was selected to allow for many frames before pixels saturate and to avoid relying exclusively on high dark currents, which would not be feasible for all arrays.

Figures 9(a) and 9(b) show the histograms of the percentage of outgoing current shared to the four direct neighbors and the four diagonal neighbors, respectively. In each figure, the median for each direction is shown in the legend, and the vertical dashed line represents the overall median of the four included directions. All histograms for the nearest neighbors overlap, which is expected as there should be no preferred sharing direction. The same behavior is also observed for the amplitude of diagonal sharing. Measurements from both arrays show about 12% to 13% of the outgoing current is shared with each of the direct nearest neighbors and about 3% to 4% of the outgoing current is shared with each of the diagonals.

Adding up the percentage of outgoing current shared to all eight nearest neighbors gives a total percentage shared, and this value is plotted for all analyzed central pixels in Fig. 9(c), where the measurements are combined into 10 e-/s wide bins and the median of these bins are plotted.

The measured low sharing values at high currents are caused by accidentally measuring tunneling dark currents in the central pixel. These tunneling currents decay as the reverse bias decreases, leading to an overestimate of the outgoing current, and a subsequent underestimate of the amount of current shared. A similar process, in reverse, applies for the low current end of H2RG-20126, where the signal rate for several pixels is sampled too close to saturation, leading to an underestimate of the outgoing current and subsequent overestimate of the amount of sharing. In between these two limits, the median values remain essentially flat, suggesting no evidence of a reciprocity-type failure of decreasing percentage of sharing with increasing current and suggest a value of total sharing to the eight immediate neighbors on the order of 60% of the outgoing current.

In general, disentangling all nearest-neighbor interactions, which are characterized by pixels sharing signal with their neighbors, is a bit complicated. This measurement, however, includes no contribution from IPC, because the voltage of the central pixel is not changing appreciably once saturated. In addition, any sharing through BF1 should be approximately the same before and after saturation, due to the limited change in depletion region width in the small voltage range across the sampled points, and as a result its contribution should be subtracted out in this measurement process. Changes in signal rate beyond the eight immediate neighbors of a BF2 sharing pixel are observed, but these changes could be caused by any combination of nearest-neighbor interactions, so the 60% value measured here serves as an underestimate of the total amount of current shared through BF2. For example, a neighboring pixel of a BF2 sharing pixel is expected to share some of its increasing signal rate with its neighbors through IPC because its voltage is changing. Similarly, the decreasing depletion region width would lead to an increase in sharing through BF1. Independent characterization of each of the nearest-neighbor interactions is required to determine the dominant mechanisms behind these long range interactions.

This large amplitude of sharing provides further evidence supporting the driving BF2 mechanism to be diffusion of the outgoing current to neighbors, rather than radiative recombination causing the saturated pixel to emit light. The latter explanation would require more than 60% of the outgoing current to radiatively recombine despite the existing evidence that recombination in general is a small contributing factor to the overall behavior, with radiative recombination making up a small portion of the overall recombination rate in HgCdTe.

It is difficult to determine where the remaining 40% of the outgoing current goes. Long range interactions are observed, but precise measurements are challenging for a few reasons. First, to eliminate the possibility of measuring signal rate changes from other long range interactions, valid central pixels for measurement must be the only saturated pixel in the 9×9 pixel box surrounding it, compared to the 5×5 boxes used for nearest-neighbor interactions. This change drastically reduces the number of measurement opportunities. In addition, each individual measurement is more easily influenced by noise because of the smaller amplitudes of long range interactions. This combination of a smaller number of noisier measurements makes arriving at clear conclusions about the amplitude of long range interactions especially problematic for individual arrays.

Interactions across a one-pixel gap are unlikely to explain the entirety of the missing 40%, however. There are 16 pixels in the 5 pixel $\times$ 5 pixel boundary surrounding the 3×3 pixel grid of nearest-neighbor interactions. For 40% of the outgoing current to go that layer, each pixel would need to receive an average of 2.5% of the outgoing current. Using the pixel shown in Fig. 2(a) as an example of the expected magnitudes, the direct long range neighbor to the west of the saturated pixel receives 0.93% of the outgoing current. Pixels in the other three cardinal directions see similar changes in magnitude but are less ideal measurement candidates because of their proximity to other saturated pixels. Assuming all 16 pixels in this long range boundary receive similar levels of current sharing, less than half of the missing 40% are accounted for. Interactions longer than two pixels away are possible, but loss of charges due to recombination at these distances is more likely.

With long range interactions unable to explain the entirety of the missing 40%, there are a few remaining possibilities. Two likely explanations are a loss of charges due to recombination and a

loss at a metal contact near the substrate. It is also possible a decrease of the dark current as pixels saturate could act as a consistent bias by overestimating the outgoing current and producing a skewed underestimate of the amount of sharing. If the sharing is driven by the LED mechanism, the missing 40% could be explained if both the charge-to-photon conversion efficiency and internal QE are <100%. As explained in Fig. 8, the internal QE is likely close to 100%, so under the LED assumption, the missing 40% could be explained by a charge-to-photon conversion efficiency of around 70%. Because charges are more likely, on average, to travel the full distance between pixels before recombining and because of the existing evidence against radiative recombination being a dominant factor in HgCdTe detectors, a conversion efficiency this large is not expected, making the LED explanation a less likely source.

Because BF2 is not exclusively a 10-μm H2RG issue but has the potential to affect a wide variety of detectors based on the *p*-*n* architecture, it is important to study its contributions with more detail to develop an appropriate correction method. This effect can largely be avoided by operating far from the full well depth, but there are some situations where BF2 will be inescapable. Fortunately, the only truly unavoidable case allows for a simple, rudimentary correction method.

In HgCdTe arrays, there is a small group of inoperable pixels with extremely elevated dark currents that saturate within the pedestal frame and, as a result, share current with their neighbors by BF2 throughout the entire integration time. The prevalence of these pixels increases with increasing cutoff wavelength because the softer material is more susceptible to the defects facilitating these high trap-assisted tunneling currents.

H2RG-20126, for example, has 33,975 of such pixels, representing 0.8% of the array. All eight neighbors of these troublesome pixels would appear anomalously brighter than their neighbors due to their interactions with the central pixel. Because this sharing is localized around a certain class of inoperable pixels, which preferentially clump together along cross-hatching lines, the impact will be largest on certain sections of the array. This will be especially problematic for missions attempting to perform precise spectrometry, such as those designed to measure the small wavelength-dependent variations in transit depths, because certain wavelengths will consistently and incorrectly appear brighter due to the location on the array where they are detected, even if the inoperable central pixels are masked. Masking the neighbors of this group of inoperable pixels to remove the influence of BF2 requires a factor as large as 9 increase to cover the central pixel and each of its neighbors, representing a total loss of up to 7.2% of the array area to avoid BF2.

Rather than to remove so many otherwise operable pixels from contributing to scientific data, it would be preferable to correct for the effect in a meaningful way. Because the central pixels are sharing throughout the full integration time, a simple approximate calculation can be performed. From Fig. 9, the expected sharing to each of the direct neighbors is about 12% of the outgoing current and is 3% to the diagonal neighbors. As a result, the direct neighbors see ~112% of the photocurrent throughout the integration time, and the diagonal neighbors see 103%. This approximation ignores sharing of the central pixel's dark current, so it is more accurate as the photocurrent increases.

Assuming the BF2 measurements for an arbitrary array shows that the fraction of current sent to the direct neighbors is γ_1 and the fraction sent to the diagonals is γ_2, then the simple corrected signals for the neighbors N and diagonals D can be calculated as

$$N = \frac{S_N}{1+\gamma_1} \qquad D = \frac{S_D}{1+\gamma_2}, \tag{5}$$

where S_N and S_D are the measured signals for the neighbor and diagonals after nonlinearity correction, respectively. Similarly, because the excess signal that has now been removed from the neighbors came from the central pixel, it can be restored there, giving an approximate estimate of the photocurrent hitting the central pixel, and its corrected measured value C would be

$$C = \frac{1}{4(\gamma_1+\gamma_2)}\left(\sum_{i=1}^{4}\frac{\gamma_1 S_{N,i}}{1+\gamma_1} + \sum_{j=1}^{4}\frac{\gamma_2 S_{D,j}}{1+\gamma_2}\right), \tag{6}$$

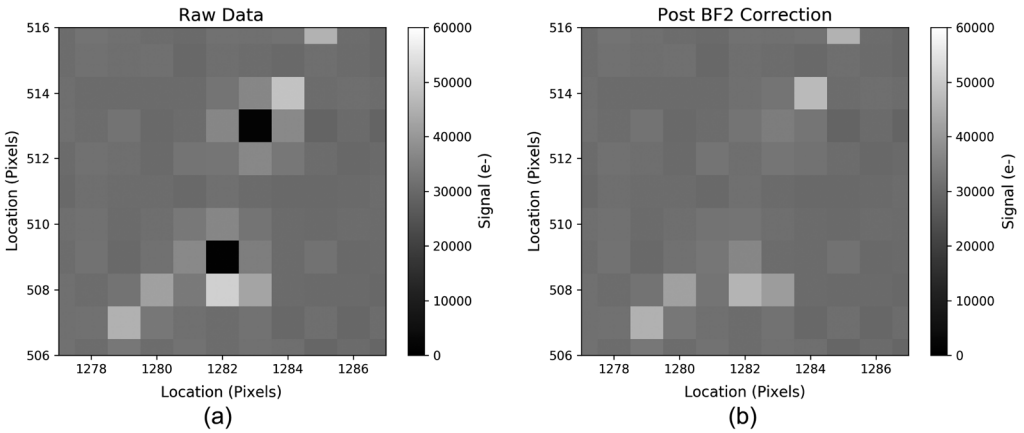

Fig. 10 An example of the BF2 correction for weakly illuminated neighbors of pixels that saturate during the pedestal frame. (a) CDS image in dim illumination showing two instances of BF2. The pixels in black are those with dark currents large enough to saturate before the pedestal frame is read. As these pixels are saturated prior to the integration period, they accumulate no charge during the integration period and appear as black "dead" pixels. The neighbors of these pixels are anomalously bright, exhibiting the characteristic plus-sign signature of a nearest-neighbor interaction because of sharing through BF2. (b) The result of performing the BF2 correction. The majority of the inhomogeneity caused by BF2 is removed and the signal values of the neighboring pixels match the background signal level.

where the sum over i covers the four direct neighbors and the sum over j covers the four diagonal neighbors. The result of this correction, under low illumination where the approximations used are weakest, is shown in Fig. 10. Although showing promising results, this correction should serve principally as a proof of concept for the possibility of a stronger correction method that does not rely on an approximation.

Corrections for other situations, which will be more important for missions with longer integration times, will be significantly more challenging, if not infeasible, because the behavior in any integration time will be extremely situation dependent.

A more elegant solution will likely come from an iterative deconvolution[21] with a nearest-neighbor matrix, such as has been proposed for correcting IPC. Populating a matrix such as this requires decoupling each nearest-neighbor interaction from the others to study their behavior independently. This task is currently being pursued using the following lengthy process. First, using single pixel resets where a central pixel can be reset to a different voltage without altering the voltage across any of the neighbors, the IPC contributions can be measured. Because IPC is a completely voltage driven effect, when these single pixel resets are performed in the dark, any change in the neighboring pixels above the background when the center pixel is reset to a different voltage must be attributable to IPC, and not BF1 or BF2. This experiment must be repeated for a variety of different reset signal and background levels to fully characterize the behavior of the coupling coefficients for IPC. Once IPC is characterized and removed, BF1 can be studied using single pixel resets under illumination, where the increase in signal rates in neighbors of bright pixels as the difference in signal value between neighboring pixels increases must be due to BF1. Finally, once IPC and BF1 can be corrected, disentangled measurements of BF2 can be performed. Combining these separate measurements will give useful information on how these nearest neighbor interactions scale with different variables, a crucial step in developing meaningful nearest-neighbor corrections.

5 Summary

Laboratory measurements are performed to investigate an additional nearest-neighbor interaction that is similar in nature to the brighter-fatter effect, in that it makes brighter sources appear fatter than dimmer sources, and to the blooming observed in CCDs. This effect is characterized by a pixel spilling over and sending current to its neighbors as it approaches saturation and is

caused by a sharing of the outgoing current that increases exponentially until becoming equal and opposite to the incoming current at saturation. Approximately 12% to 13% of this current is shared to each of the nearest neighbors and an additional 3% to 4% is shared to each of the diagonal neighbors. This measurement is independent of other nearest-neighbor interactions, such as IPC, but only covers sharing to the immediate eight pixels surrounding a saturated central pixel, suggesting the total percent of the outgoing current shared is greater than 60%. The most likely mechanism of current sharing is pure lateral diffusion of charges from the central pixel to a neighbor's depletion region, rather than radiative recombination turning the pixel into a LED because of the expected small number of recombination events as a charge travels between two pixels and the preference for nonradiative recombination methods in HgCdTe. The LED option as a possible cause of this behavior cannot be definitively eliminated, however.

Although the majority of this effect can be avoided by operating far from full wells, there are a few pixels with trap-assisted tunneling dark currents large enough to cause a pixel to saturate without illumination in short integration times. For these pixels, this effect will be unavoidable. In addition, because these pixels preferentially lie in localized areas of the array, this brighter-fatter type effect can play an outsize role in missions attempting to perform spectroscopy because it will cause certain wavelengths to appear anomalously bright, even if the central saturated pixel is blocked from contributing to the scientific data. For future missions planning to characterize exoplanet atmospheres, for example, this effect runs the risk of reducing measured transit depths at certain wavelengths, potentially masking some of the minuscule variations required to detect a crucial absorption feature. Blocking the immediate neighbors of these pixels can lead to a factor of 9 increase in the unusable area of the array, so a correction method is significantly preferable. A preliminary, proof-of-concept correction method is detailed and the next steps to improve the correction and measure the contributions from three nearest-neighbor interactions is also described.

Acknowledgments

Funding for this work was received from Cornell University through New York Space Grant No. 80NSSC20M0096, the Jet Propulsion Laboratory through the Near Earth Object Camera (NEOCam) Extended Phase A Subcontract 1573311, and the University of Arizona through the Near Earth Object Surveillance Mission (NEOSM) Extended Phase A Grant No. 80MSFC20C0045. The authors would also like to thank Peter Eisenhardt of the Jet Propulsion Laboratory for his contributions to this work. In addition, the authors would like to thank the referees for their constructive feedback and support in strengthening this paper.

References

1. A. C. Moore, Z. Ninkov, and W. J. Forrest, "Interpixel capacitance in nondestructive focal plane arrays," *Proc. SPIE* **5167**, 204–215 (2004).
2. P. Antilogus et al., "The brighter-fatter effect and pixel correlations in CCD sensors," *J. Instrum.* **9**, C03048 (2014).
3. A. A. Plazas et al., "Laboratory measurement of the brighter-fatter effect in an H2RG infrared detector," *Publ. Astron. Soc. Pac.* **130**, 065004 (2018).
4. A. Plazas et al., "Nonlinearity and pixel shifting effects in HXRG infrared detectors," *J. Instrum.* **12**, C04009 (2017).
5. Y. Chang et al., "Surface morphology and defect formation mechanisms for $HgCdTe_{(211)}B$ grown by molecular beam epitaxy," *J. Electron. Mater.* **37**(9), 1171–1183 (2008).
6. M. Carmody et al., "Molecular beam epitaxy grown long wavelength infrared HgCdTe on Si detector performance," *J. Electron. Mater.* **34**(6), 832–838 (2005).
7. M. Martinka et al., "Characterization of cross-hatch morphology of MBE (211) HgCdTe," *J. Electron. Mater.* **30**(6), 632–636 (2001).
8. M. S. Cabrera et al., "Development of 13 μm cutoff HgCdTe detector arrays for astronomy," *J. Astron. Telesc. Instrum. Syst.* **5**(3), 036005 (2019).
9. A. M. Fowler and I. Gatley, "Demonstration of an algorithm for read-noise reduction in infrared arrays," *Astrophys. J.* **353**, L33 (1990).

10. J. D. Garnett and W. J. Forrest, "Multiply sampled read-limited and background-limited noise performance," *Proc. SPIE* **1946**, 395–404 (1993).
11. L. Mortara and A. Fowler, "Evaluations of charge-coupled device (CCD) performance for astronomical use," *Proc. SPIE* **0290**, 28–33 (1981).
12. K. Donlon, Z. Ninkov, and S. Baum, "Signal dependence of interpixel capacitance in hybridized HgCdTe H2RG arrays for use in James Webb space telescope's NIRcam," *Proc. SPIE* **9915**, 807–814 (2016).
13. G. R. Zengilowski et al., "Signal nonlinearity measurements and corrections in MWIR and LWIR HgCdTe H2RG arrays for NEO surveyor," *Proc. SPIE* **11454**, 616–633 (2020).
14. W. Shockley, "The theory of p-n junctions in semiconductors and p-n junction transistors," *Bell Syst. Tech. J.* **28**(3), 435–489 (1949).
15. J. E. Hubbs et al., "Lateral diffusion length changes in HgCdTe detectors in a proton environment," *IEEE Trans. Nucl. Sci.* **54**(6), 2435–2443 (2007).
16. H. Cui et al., "Analysis of the mechanisms of electron recombination in HgCdTe infrared photodiode," *Opt. Quantum Electron.* **45**(7), 629–634 (2013).
17. G. Qiu et al., "Minority carrier lifetimes in different doped LWIR HgCdTe grown by LPE," *Proc. SPIE* **8419**, 313–318 (2012).
18. M. A. Kinch et al., "Minority carrier lifetime in p-HgCdTe," *J. Electron. Mater.* **34**(6), 880–884 (2005).
19. V. C. Lopes, A. J. Syllaios, and M. C. Chen, "Minority carrier lifetime in mercury cadmium telluride," *Semicond. Sci. Technol.* **8**, 824–841 (1993).
20. B. J. Rauscher et al., "James webb space telescope near-infrared spectrograph: dark performance of the first flight candidate detector arrays," *Proc. SPIE* **7021**, 641–659 (2008).
21. K. Donlon, Z. Ninkov, and S. Baum, "Point-spread function ramifications and deconvolution of a signal dependent blur kernel due to interpixel capacitive coupling," *Publ. Astron. Soc. Pac.* **130**, 074503 (2018).

Biographies of the authors are not available.